

# Parametric amplification and oscillation with walkoff-compensating crystals

D. J. Armstrong, W. J. Alford, T. D. Raymond, and A. V. Smith

*Department of Lasers, Optics, and Remote Sensing, Sandia National Laboratories, Albuquerque, New Mexico 87185-1423*

M. S. Bowers

*Aculight Corporation, Suite 100, 40 Lake Bellevue, Bellevue, Washington 98005*

Received April 5, 1996; revised manuscript received July 24, 1996

We measure and model parametric gain and oscillation for two crystals arranged for walkoff compensation. We show how the orientation of the crystals determines the relative sign of the nonlinear mixing coefficient in the two crystals. This sign dramatically influences small signal gain and oscillator performance, and we show how to determine the correct crystal orientation from parametric-gain measurements. The performance of two-crystal oscillators is examined with particular attention to beam tilts, conversion efficiency, and beam quality. We find reduced efficiency and increased oscillation threshold when the coefficients have opposite signs in a two-crystal ring oscillator. Sign reversal seems to have little influence on spectral purity or far-field beam profiles when the oscillator is seeded. © 1997 Optical Society of America [S0740-3224(97)00202-6]

## 1. INTRODUCTION

Birefringent nonlinear crystals are widely used to convert the wavelength of laser light by second-harmonic generation, sum- or difference-frequency mixing, and parametric processes. When the propagation directions of the interacting waves do not lie along an optic axis of the crystal, extraordinary rays undergo birefringent walkoff while ordinary rays do not. Because birefringent phase matching relies on the presence of both ordinary and extraordinary waves, walkoff is often a concern, particularly for small-diameter beams, where it limits the length of beam overlap in the crystal and often limits conversion efficiency. This can be partially counteracted by pairs of crystals arranged in a walkoff-compensated orientation,<sup>1-11</sup> where the walkoff direction is reversed in the second crystal of each pair. This arrangement has the added advantage that the beams do not translate if the crystal angles are synchronously adjusted to tune the phase-matched wavelength. Walkoff compensation also increases the acceptance angle for mixing relative to a single crystal of the same overall length.<sup>12</sup>

Sometimes overlooked in the use of multiple crystals is the importance of the relative signs of the effective nonlinear coefficients for the two crystals, as well as the intercrystal phase shifts of the mixing waves caused by dispersion of air and by antireflection coatings on the crystals. An extreme example of the importance of these factors is two identical crystals, perfectly phase matched, with no intercrystal phase shift. If the nonlinear coefficients have opposite signs, the net effect of mixing is to leave the incident waves unaltered. That is, mixing in the second crystal exactly cancels the mixing in the first crystal. The effects of the phase and the relative signs of the nonlinear coefficient have been discussed by Harris for parametric mixing,<sup>13</sup> by Andreev *et al.*<sup>5</sup> for general fre-

quency conversion, and in detail by Zondy *et al.*<sup>10,11</sup> for second-harmonic generation.

In this paper we describe parametric gain and oscillation for two-crystal configurations, paying particular attention to the relative signs of the nonlinear coefficients, the intercrystal phase shifts, and the effects of phase mismatch,  $\Delta k$ , in the two crystals. We show how to determine the relative signs of the nonlinear coefficients and how to adjust them. We demonstrate the use of intercrystal phase shifts or imperfect phase matching to overcome the gain cancellation implied by reversed coefficients to produce net parametric gain. We also show how walkoff compensation increases the acceptance angle for gain. We compare our laboratory measurements of parametric gain in  $\text{KTiOPO}_4$  (KTP) crystals under various conditions with calculations and discuss the implications for parametric oscillators. This analysis is supported by experimental observations and theoretical modeling of a two-crystal, KTP optical parametric oscillator (OPO). We show that under certain conditions, the two-crystal devices exhibit spectral and modal properties absent in single-crystal oscillators.

## 2. PARAMETRIC-GAIN EQUATIONS

We begin with an analytic description of parametric mixing in the plane-wave approximation neglecting pump depletion. This low-gain limit accurately describes our two-crystal, single-pass gain measurements, and is useful for understanding the effects of phase mismatch, crystal orientation, and intercrystal phase near the oscillation threshold in an OPO. Parametric oscillation will be treated with a more general numerical model in a later section.

### A. Single-Crystal Gain

In the approximation of quadratic nonlinearity the nonlinear polarizations may be written in the form

$$P_j(\omega_3) = \chi_{j,k,l}^{(2)}(-\omega_3; \omega_1\omega_2)E_k(\omega_1)E_l(\omega_2), \quad (1)$$

where  $j$ ,  $k$ , and  $l$  refer to polarization directions associated with the fields at frequencies  $\omega_3$ ,  $\omega_1$ , and  $\omega_2$ , respectively. For a chosen propagation direction and set of polarizations this can be written in the simplified form

$$P(\omega_3) = 2\varepsilon_0 d_{\text{eff}} E(\omega_1)E(\omega_2). \quad (2)$$

When this nonlinear polarization is included in Maxwell's equations, the result is the nonlinear mixing equations presented in numerous textbooks on nonlinear optics.<sup>14-16</sup> Neglecting linear absorption, in SI units they are

$$\frac{d\varepsilon_s}{dz} = i \frac{d_{\text{eff}}}{c} \frac{\omega_s}{n_s} \varepsilon_p \varepsilon_i^* \exp(i\Delta kz), \quad (3)$$

$$\frac{d\varepsilon_i}{dz} = i \frac{d_{\text{eff}}}{c} \frac{\omega_i}{n_i} \varepsilon_p \varepsilon_s^* \exp(i\Delta kz), \quad (4)$$

$$\frac{d\varepsilon_p}{dz} = i \frac{d_{\text{eff}}}{c} \frac{\omega_p}{n_p} \varepsilon_s \varepsilon_i \exp(-i\Delta kz), \quad (5)$$

where the electric field  $E_\omega$  at frequency  $\omega$  is given by

$$E_\omega = \frac{1}{2} \{ \varepsilon_\omega \exp[-i(\omega t - k_\omega z)] + \varepsilon_\omega^* \exp[i(\omega t - k_\omega z)] \}, \quad (6)$$

the phase velocity mismatch  $\Delta k$  is defined by

$$\Delta k = k_p - k_s - k_i, \quad (7)$$

and

$$\omega_p = \omega_s + \omega_i. \quad (8)$$

As is customary, the subscripts  $p$ ,  $s$ , and  $i$  refer to pump, signal, and idler, respectively, and the coefficient  $d_{\text{eff}}$  is the effective nonlinearity expressed in units of m/V. In this section we assume that the pump field is much stronger than the signal and idler fields and that pump depletion is negligible. The solution of Eqs. (3), (4), and (5) for the growth of signal and idler fields for a single crystal is<sup>16</sup>

$$\begin{aligned} \varepsilon_s(z) = & \varepsilon_s(0) \left( \cosh \gamma z - \frac{i\Delta k}{2\gamma} \sinh \gamma z \right) \exp\left(\frac{i\Delta kz}{2}\right) \\ & + i \frac{A}{\gamma} \varepsilon_i^*(0) \sinh \gamma z \exp\left(\frac{i\Delta kz}{2}\right), \end{aligned} \quad (9)$$

$$\begin{aligned} \varepsilon_i^*(z) = & \varepsilon_i^*(0) \left( \cosh \gamma z + \frac{i\Delta k}{2\gamma} \sinh \gamma z \right) \exp\left(\frac{-i\Delta kz}{2}\right) \\ & - i \frac{B}{\gamma} \varepsilon_s(0) \sinh \gamma z \exp\left(\frac{-i\Delta kz}{2}\right), \end{aligned} \quad (10)$$

where  $A$ ,  $B$ , and  $\gamma$  are constants defined as

$$A = \frac{d_{\text{eff}} \omega_s \varepsilon_p}{c n_s}, \quad (11)$$

$$B = \frac{d_{\text{eff}} \omega_i \varepsilon_p^*}{c n_i}, \quad (12)$$

$$\gamma = \frac{1}{2} \sqrt{4AB - \Delta k^2}. \quad (13)$$

If the idler field is initially zero [ $\varepsilon_i(0) = 0$ ], the signal field grows as

$$\varepsilon_s(z) = \varepsilon_s(0) \left( \cosh \gamma z - \frac{i\Delta k}{2\gamma} \sinh \gamma z \right) \exp\left(\frac{i\Delta kz}{2}\right). \quad (14)$$

We define the signal gain in a crystal of length  $L$  as

$$G_s = \left| \frac{\varepsilon_s(L)}{\varepsilon_s(0)} \right|^2 - 1. \quad (15)$$

### B. Two-Crystal Gain

Parametric gain for two crystals can be derived from Eqs. (9) and (10) in a straightforward manner by use of the output fields from the first crystal as inputs for the second. The only subtlety is realizing that the phases deduced from Eqs. (9) and (10) are only the phases added by the nonlinear interaction. Before use of the fields as input to the second crystal, the phase shifts due to linear propagation,  $\exp(ik_\omega L)$ , which were coalesced into the  $\pm i\Delta kz$  exponents in Eqs. (3)–(5), must be restored. In addition, the intercrystal phase shift must be added. This is actually a relative phase shift defined by  $\theta = \phi_p - \phi_s - \phi_i$ , where the  $\phi$  parameters are intercrystal phase shifts of the individual waves. The phases can be properly accounted for by increasing the phase of the pump field by  $\Delta k_1 L_1 + \theta$  or equivalently by decreasing the phase of either the signal or the idler field by the same amount. Then the expression for the signal output field from two crystals of lengths  $L_1$  and  $L_2$  is

$$\begin{aligned} \varepsilon_s = & \varepsilon_s(0) \exp(i\Delta k_1 L_1/2 + i\Delta k_2 L_2/2) \\ & \times \left[ \cosh \gamma_1 L_1 \cosh \gamma_2 L_2 \right. \\ & - \frac{\Delta k_1 \Delta k_2}{4 \gamma_1 \gamma_2} \sinh \gamma_1 L_1 \sinh \gamma_2 L_2 \\ & + \frac{A_2 B_1}{\gamma_1 \gamma_2} \sinh \gamma_1 L_1 \sinh \gamma_2 L_2 \exp(i\theta) \\ & - i \frac{\Delta k_1}{2 \gamma_1} \sinh \gamma_1 L_1 \cosh \gamma_2 L_2 \\ & \left. - i \frac{\Delta k_2}{2 \gamma_2} \cosh \gamma_1 L_1 \sinh \gamma_2 L_2 \right] \\ & + \varepsilon_i^*(0) \exp(i\Delta k_1 L_1/2 + i\Delta k_2 L_2/2) \\ & \times \left[ \frac{A_1 \Delta k_2}{2 \gamma_1 \gamma_2} \sinh \gamma_1 L_1 \sinh \gamma_2 L_2 \right. \\ & - \frac{A_2 \Delta k_1}{2 \gamma_1 \gamma_2} \sinh \gamma_1 L_1 \sinh \gamma_2 L_2 \exp(i\theta) \\ & + i \frac{A_1}{\gamma_1} \sinh \gamma_1 L_1 \cosh \gamma_2 L_2 \\ & \left. + i \frac{A_2}{\gamma_2} \cosh \gamma_1 L_1 \sinh \gamma_2 L_2 \exp(i\theta) \right], \end{aligned} \quad (16)$$

where subscripts 1 and 2 refer to the first and second crystals. The expression for the idler field is similar. Note that the intercrystal phase,  $\theta$ , and the second crystal coefficient,  $A_2$ , always appear together as  $[A_2 \exp(i\theta)]$  in the expression for the signal field. Similarly,  $\theta$  and  $B_2$  always appear together in the expression for the idler field. Thus reversing the sign of  $d_{\text{eff}}$  in the second crystal, and hence of  $A_2$  and  $B_2$ , is equivalent to an intercrystal phase shift of  $\theta = \pi$ .

Figure 1(a) is a plot of the two-crystal signal gain,  $G_s$ , as defined by Eq. (15), for two crystals each of length  $L$  with  $d_{\text{eff}}$  values of equal magnitude. In this example, the  $d_{\text{eff}}$  values have the same sign,  $L = 10$  mm,  $\varepsilon_i(0) = 0$ ,  $\theta = 0$ , and  $\Delta k_1, \Delta k_2$  cover a range of values. A value of  $A_1 B_1 = A_2 B_2 = 7.47 \times 10^3 \text{ m}^{-2}$  was selected to give a peak gain of approximately 7.5. The gain surface is plotted on a grid in dimensionless units of  $\Delta k_1 L / \pi$ ,  $\Delta k_2 L / \pi$ . We will refer to this case where the signs of the  $d_{\text{eff}}$  values are the same, and  $\theta = 0$  or, equivalently, where the signs of the  $d_{\text{eff}}$  values are opposite, and  $\theta = \pi$ , as the *correct orientation*. Figure 1(b) is a plot of the same, except with opposite signs for  $d_{\text{eff}}$  in the two crystals, or, equivalently, with the same signs for  $d_{\text{eff}}$  and an intercrystal phase shift of  $\pi$ . We will call this case the *incorrect orientation*. It is easy to show from Eq. (16) that for the incorrect orientation there is no gain along the line  $\Delta k_1 = -\Delta k_2$ . That is, in the diagonal valley through the point  $\Delta k_1 = \Delta k_2 = 0$ , gain is zero. The

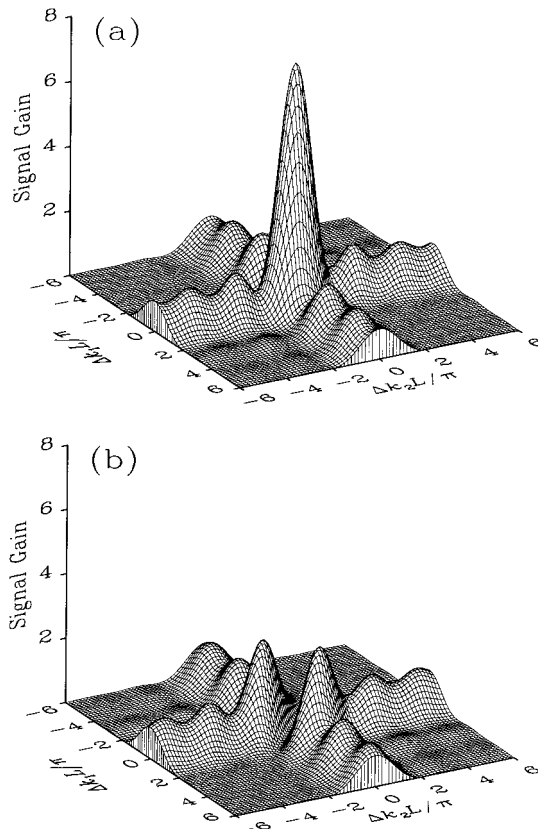


Fig. 1. Two-crystal, single-pass parametric gain calculated from Eq. (16) for identical crystals with  $\varepsilon_i(0) = 0$  and  $A_1 B_1 = A_2 B_2 = 7.47 \times 10^3 \text{ m}^{-2}$  with  $d_{\text{eff}}$  values of (a) the same sign and (b) opposite signs.

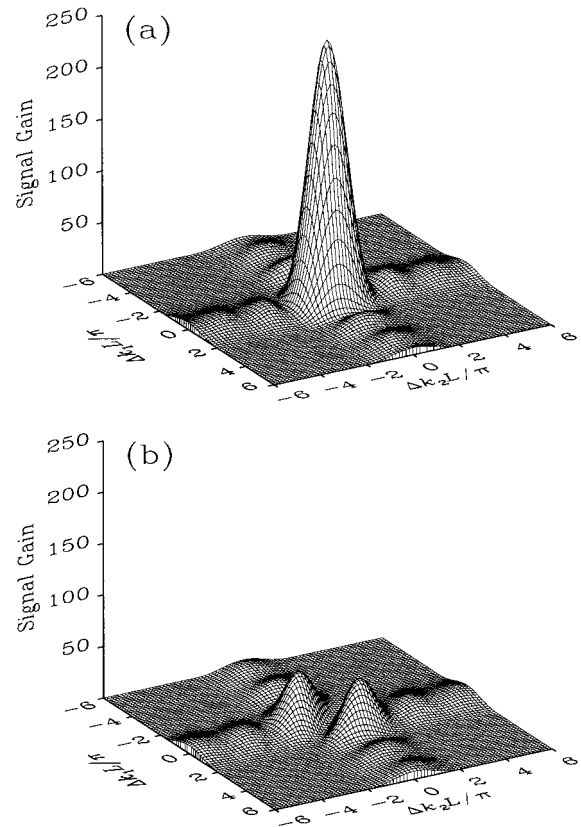


Fig. 2. Same as Fig. 1 but with  $A_1 B_1 = A_2 B_2 = 2.99 \times 10^4 \text{ m}^{-2}$ .

points of maximum gain lie along the diagonal  $\Delta k_1 = \Delta k_2$  and are located at  $\Delta k L / \pi \approx 1$ . The maximum gain in this case, however, is substantially smaller than that for the correct orientation. Note that in both cases the gain far from the origin is significant only when either  $\Delta k_1$  or  $\Delta k_2$  is near zero. In this limit the crystals are nearly decoupled, and the gain is due primarily to the single crystal that is nearly phase matched.

Figure 2 shows how these gain surfaces change character as the parametric gain is increased. Here the values of  $A_1 B_1$  and  $A_2 B_2$  are increased to  $2.99 \times 10^4 \text{ m}^{-2}$  to give a peak gain of approximately 250. The side lobes become less significant relative to the central peak(s), and the ratio of the peak gain for the correct orientation to that for the incorrect orientation increases. Additionally, the position of maximum gain in the incorrect case shifts to slightly larger values of  $\Delta k$ .

Although we do not show the surfaces here, we studied the transition from the incorrect to the correct orientation by keeping the signs of the  $d_{\text{eff}}$  values the same and varying  $\theta$  from  $\pi$  to zero. As expected, the surface transforms smoothly between the two cases shown, with one of the central peaks growing relative to the other and moving toward the origin.

### 3. SIGNS OF $d_{\text{eff}}$

The dramatic difference between the gain surfaces of Figs. 1(a) and 1(b) emphasizes the importance of the intercrystal phase shift and the relative signs of  $d_{\text{eff}}$  for two-

crystal devices. Two factors determine the sign of  $d_{\text{eff}}$  for a particular crystal and mixing process. One is the cut of the crystal relative to the crystallographic axes; the other is the laboratory orientation of the crystal. Figure 3 shows the four useful laboratory orientations of a crystal. It shows that any crystal can be rotated about either of two axes to reverse the walkoff direction. We address here the less obvious effect of these rotations on the sign of  $d_{\text{eff}}$ . We will show that for a mixing process involving an odd number of waves with extraordinary polarization, all four combinations of walkoff direction (left or right) and sign of  $d_{\text{eff}}$  (+ or -) can be achieved by crystal rotations. For mixing processes involving an even number of waves of extraordinary polarization, the reversal of walkoff direction by rotation of the crystal is always accompanied by a reversal of the sign of  $d_{\text{eff}}$ , so the walkoff direction and the sign of  $d_{\text{eff}}$  cannot be independently reversed. In this case the crystallographic cut of the crystals can be used to adjust the sign of  $d_{\text{eff}}$ . We will give examples showing how the proper cuts can be selected.

Consider first how the laboratory orientation of identically cut crystals affects the sign of  $d_{\text{eff}}$  and the walkoff

direction. This can be done by manipulating the nonlinear susceptibility tensor for the crystal,<sup>10</sup> or, as we show here, it can be deduced directly from the overall symmetry of the crystal, the optical fields, and the nonlinear polarization as long as the longitudinal fields and polarization are insignificant. Phase matching along a particular propagation direction in a birefringent crystal occurs only for a specific set of polarization directions for the three waves. Each wave will be either ordinary or extraordinary as determined by the phase-matching requirement. Thus any interaction can be designated by ooe, oeo, oee, ..., where o refers to ordinary, and e to extraordinary polarization directions, and the first letter designates the nonlinear polarization induced by the applied optical fields associated with the last two letters.

In Fig. 3 we examine the symmetry properties for an eoo process. The baseline case is shown in (a), while (b), (c), and (d) show the crystal rotated about each of the three orthogonal axes, indicated by the dashed lines. The light propagates from the left to the right crystal face. The line on the top of the crystal indicates the orientation of the crystal's optic axis. This is also the direction of walkoff for positive uniaxial crystals or opposite the walkoff direction for negative uniaxial crystals. All orientations in (a)–(d) have the same phase mismatch  $\Delta k$ . Let the two arrows labeled o represent the two input fields at some points in the crystal at some instant in time. The arrow labeled e represents the induced extraordinary polarization. In (a), two up input fields induce an out-of-the-page polarization. In (b) the crystal, fields, and induced polarization have been rotated about an out-of-the-page axis so the walkoff direction is opposite the baseline case. The physical process represented by the arrows is the same as in (a) because in the reference frame of the crystal nothing has changed. In the laboratory reference frame, however, two down fields now induce an out-of-the-page polarization. Thus two sign-reversed driving fields produce the same sign polarization as in the baseline case. The polarization is related to the driving fields by  $P(\omega_3) = 2\epsilon_0 d_{\text{eff}} E(\omega_1)E(\omega_2)$  as in Eq. (2), so reversing the signs of the two  $E$  fields but not the sign of  $P$  implies that the sign of  $d_{\text{eff}}$  is unchanged. Therefore this orientation of the crystal compensates walkoff and has the same sign for  $d_{\text{eff}}$  as the baseline case.

In (c) the crystal is rotated about the vertical axis. Here, the walkoff direction is not reversed, but the fields induce an into-the-page polarization. This rotation is equivalent to changing the sign of the nonlinear polarization but not the driving fields, so the sign of  $d_{\text{eff}}$  must be opposite that of the baseline case. In (d) the crystal is rotated about the propagation axis so walkoff is compensated. This rotation is equivalent to reversing the driving fields and the polarization, so again the sign of  $d_{\text{eff}}$  must be opposite that of the baseline case.

This analysis is easily applied to other nonlinear interactions as well. Clearly the rotation of (b) reverses the direction of o fields and polarizations but not e fields. Thus the sign of  $d_{\text{eff}}$  will be reversed for processes with an odd number of o waves. The rotation of (c) reverses e fields and polarizations so  $d_{\text{eff}}$  is sign reversed only for processes with an odd number of e waves. The rotation of (d) reverses both e and o fields and polarizations so  $d_{\text{eff}}$

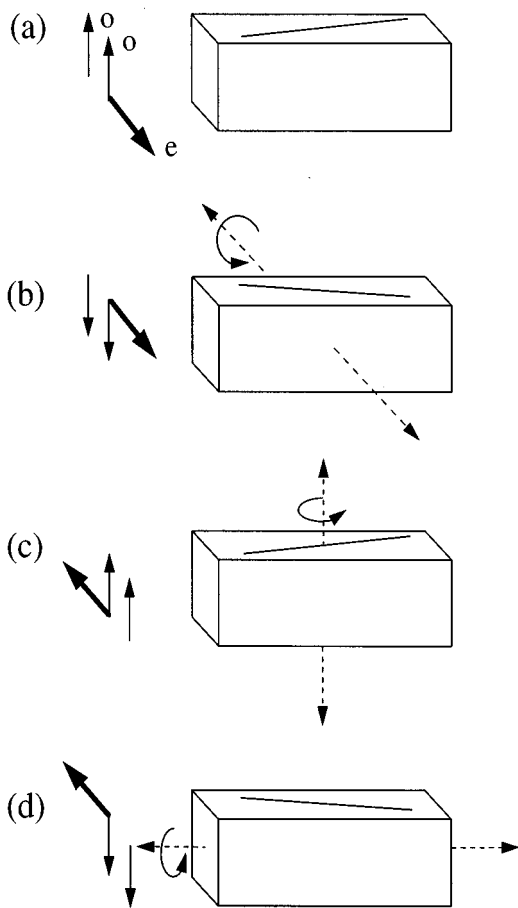


Fig. 3. Diagrams used to deduce relative signs of the  $d_{\text{eff}}$  values for various crystal orientations. The orientation labeled (a) represents the baseline case. The dashed arrows in (b), (c), and (d) indicate axes about which the crystal is rotated by  $180^\circ$ . The arrows to the left of the crystals represent the directions of the applied fields and the induced polarization. The diagonal lines on top of the crystals represent the orientation of the optic axes.

is always sign reversed. Thus we conclude that for walkoff-compensated interactions [rotations of (b) and (d)], involving one e wave, the sign of  $d_{\text{eff}}$  for the two crystals can be the same [rotation (b)] or opposite [rotation (d)], whereas for interactions with two e waves, walkoff compensation is always accompanied by a sign reversal of  $d_{\text{eff}}$ .

From this discussion it is clear that the crystallographic cut is not important for mixing with an odd number of e waves because any combination of walkoff direction and sign of  $d_{\text{eff}}$  can be achieved by applying laboratory rotations of the crystal. For mixing with an even number of e waves, this is not true because a reversal of walkoff direction is always accompanied by a change in the sign of  $d_{\text{eff}}$ . To achieve walkoff compensation with the correct orientation for the two crystals, we must either arrange a  $\pi$  phase adjustment between the crystals or use crystals with different crystallographic cuts.

Here we present two examples of the use of different cuts. In uniaxial crystals the requirement of collinear phase matching determines the angle  $\theta$  between the crystal's optic axis and the light-propagation direction. Within this double cone ( $\theta$  and  $\pi - \theta$ ) of propagation directions, the linear optical properties are independent of azimuthal angle  $\phi$  but the nonlinear properties are not. Certain values of  $\phi$ , measured relative to the crystallographic axes, maximize the value of  $d_{\text{eff}}$ . These optimal angles depend on the symmetry properties of the crystal and the nature of the mixing process.<sup>17,18</sup> Generally, either sign of  $d_{\text{eff}}$  can be achieved depending on the value of  $\phi$ . Our first example is crystals of symmetry 3m, which includes the uniaxial crystals beta barium borate and lithium niobate. For processes with two e waves the value of  $d_{\text{eff}}$  is proportional to  $\cos^2 \theta \cos 3\phi$ . This maximizes at  $\phi = 0, \pi/3, 2\pi/3, \pi, 4\pi/3, \text{ and } 5\pi/3$ . Note that the sign of  $d_{\text{eff}}$  alternates as  $\phi$  is stepped through this set, and in addition the sign and magnitude are the same for  $\theta$  and  $\pi - \theta$ . Thus a pair of crystals suitable for walkoff-compensated operation would consist of one cut at  $\phi = 0$  and one cut at  $\phi = \pi$  at the same angle  $\theta$ . When these are positioned for walkoff compensation, they will always have the same sign for  $d_{\text{eff}}$  for mixing with two e waves.

As a second example, consider crystals of symmetry mm2, which includes KTP, potassium niobate, and lithium triborate. These are biaxial crystals, so the phase-matching loci of  $\theta$  and  $\phi$  are somewhat more complex than for uniaxial crystals, as are the expressions for the effective nonlinearity. However, if we restrict the propagation directions to lie in the principle plane XY, which is the only one with nonzero  $d_{\text{eff}}$  when two e waves are used, phase matching occurs only at four values of  $\phi$ , one in each quadrant of the XY plane (at  $\phi = \phi_0, \pi - \phi_0, \pi + \phi_0, \text{ and } 2\pi - \phi_0$ ), and  $d_{\text{eff}} = d_{31} \sin^2 \phi + d_{32} \cos^2 \phi$ . The sign of  $d_{\text{eff}}$  is the same for each of the four phase-matching directions, but because walkoff is always toward the Y axis, crystals cut from adjacent quadrants will have opposite walkoff directions. These constitute walkoff-compensated pairs with the same sign of  $d_{\text{eff}}$ .

#### 4. ACCEPTANCE ANGLE

For nonlinear mixing in a critically phase-matched process in a birefringent crystal, the acceptance angle is a measure of the tolerance to tilt away from the phase-matching angle where  $\Delta k = 0$ . It is generally defined as the angle where  $\Delta k L = 2\pi$ . Angular acceptance is usually analyzed in terms of plane waves and the angular dependence of the extraordinary refractive index. For example, suppose two o waves mix to produce an e wave with the three  $k$  vectors parallel. If the process is initially phase matched, tilting the crystal in the critical plane leaves the  $k$  vectors of the o waves unaltered but changes the  $k$  vector of the e wave because its refractive index changes with crystal angle. As the crystal is tilted away from  $\Delta k = 0$ , there is a reduction in mixing efficiency. This simple description of acceptance angle fails with beams of small transverse dimension, or when more complicated phase structures are considered, because a range of transverse  $k$  vectors is present in each beam. In that case a more appropriate picture is that walkoff of the e wave introduces phase shifts associated with the lateral displacement of the structured phase front of the e wave. The equivalence of these two descriptions is most obvious for the case of three weakly interacting waves with large diameter and spherical wave fronts. As they propagate within the crystal, the e- and the o-wave phase fronts will still be spherical, but the phase fronts of the e wave will be shifted laterally toward the direction of lower refractive index by an amount equal to the product of the walkoff angle and the propagation distance. Thus different rays of the spherical e wave have phase-front spacings, or  $k$  vectors, that depend on the propagation angle, just as expected from the angular dependence of the refractive index. The  $k$  vectors are smaller for rays tilted toward the walkoff direction. In addition, the phase fronts of the three beams will no longer have a common center of curvature, so there will be position-dependent phase shifts of the e wave relative to the o waves. Analysis of these phase shifts shows that they completely account for acceptance-angle effects.

From either viewpoint we might expect that walkoff compensation would increase the acceptance angle for mixing. If the crystal positions are fixed and the three waves are tilted away from the phase-matching angle, in the plane-wave picture, the sign of  $\Delta k$  is opposite in the two crystals so the phase slippage between e and o waves in the first crystal is reversed in the second, whereas it is compounded for two crystals without walkoff compensation, or equivalently, for a single crystal of the same net length. In the wave-front displacement picture, the lateral displacement in the second crystal is in the opposite direction to that in the first so the net phase shift associated with walkoff is reduced compared with a single crystal of the same net length.

We show here that the acceptance angle is indeed increased by walkoff compensation. Figure 4(a) is a contour plot of two-crystal parametric gain computed with Eq. (16) for the correct crystal orientation in the limit of low peak gain ( $G_s = 0.1$ ). In this limit, parametric gain with the idler input set to zero is equivalent to difference-frequency mixing. Consider a collinearly phase-matched

process with o-polarized pump and idler and e-polarized signal in two crystals of length  $L$  arranged for walkoff compensation. A tilt of the e-polarized signal beam in the critical plane introduces equal magnitude but oppositely signed  $\Delta k$  values in the two crystals due to the angular dependence of the extraordinary refractive index. The o-polarized idler wave will tilt in the opposite direction to the signal wave to minimize the transverse  $\Delta k$ , but the contribution of this tilt to the total phase mismatch is negligible for all tilts considered here. Thus starting from  $\Delta k_1 = \Delta k_2 = 0$ , a tilt of the signal wave moves the operating point along the line of slope  $-1$  in Fig. 4(a) by an amount proportional to the tilt. If instead the crystals were arranged so that walkoff in the two crystals was in the same direction, a tilt of the signal wave would move the operating point along the line of slope  $+1$ . This would be equivalent to a single crystal of length  $2L$ . Figure 4(b) shows the gain for cuts through the gain surface along the lines of slope  $+1$  and  $-1$  plotted against  $\Delta k_2 L/\pi$ . The width for the latter is twice that of the former. Thus the tolerance to tilt of an e wave is twice as large for walkoff-compensating crystals as for noncompensating crystals, or equivalently, twice as large as for a single crystal of the same total length.

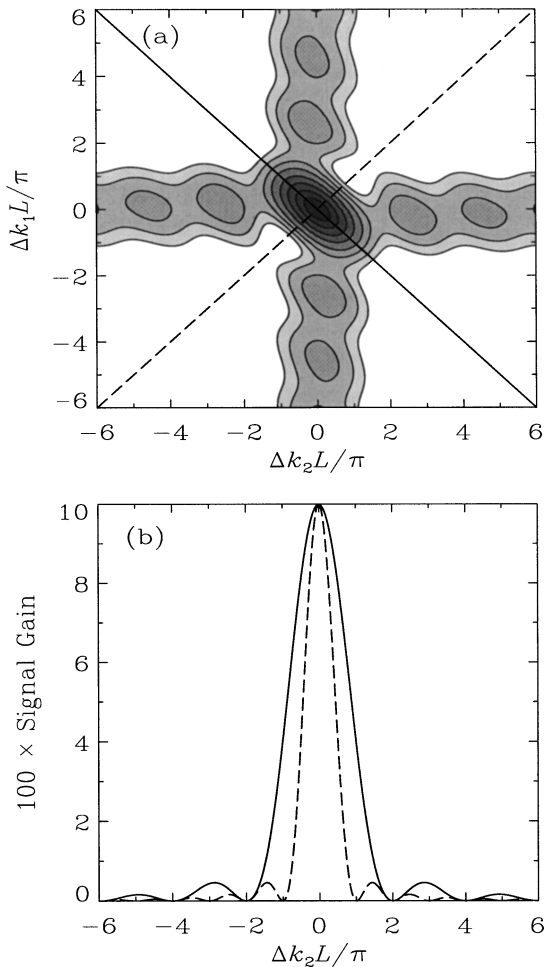


Fig. 4. (a) Contour plot of a two-crystal gain surface in the low gain limit with  $G_s = 0.1$ . (b) Cuts through the gain surface along the lines of slope  $\pm 1$ . Line styles in (b) correspond to the axes shown in (a).

In fact, in the low-conversion limit of sum- or difference-frequency generation, dividing a crystal into  $N$  segments of length  $L/N$  and arranging the segments to alternate the walkoff direction increases the tilt tolerance, or acceptance angle, by a factor of  $N$ . To illustrate this, we consider a simple plane-wave treatment of second-harmonic generation in the low-conversion limit. For a single crystal of length  $L$ , with  $\Delta k = k_{2\omega} - 2k_\omega$ , the second-harmonic field is given by

$$E_{2\omega} = \frac{\omega d_{\text{eff}}}{nc} E_\omega^2 L \frac{\sin(\Delta k L/2)}{(\Delta k L/2)} \exp(i\Delta k L/2), \quad (17)$$

and  $E_{2\omega}$  reaches zero when  $\Delta k L = 2\pi$ . If the single crystal is replaced by two walkoff-compensating crystals of length  $L/2$  where  $\Delta k_2 = -\Delta k_1$ , the harmonic field for the first crystal, including the phase shift due to linear propagation through the second crystal, is

$$E_{2\omega} = \frac{\omega d_{\text{eff}}}{nc} E_\omega^2 \frac{L}{2} \frac{\sin(\Delta k L/4)}{(\Delta k L/4)} \exp(i\Delta k L/4) \exp(-i\Delta k L/2) \quad (18)$$

and for the second crystal

$$E_{2\omega} = \frac{\omega d_{\text{eff}}}{nc} E_\omega^2 \frac{L}{2} \frac{\sin(\Delta k L/4)}{(\Delta k L/4)} \exp(-i\Delta k L/4). \quad (19)$$

The sum of these is

$$E_{2\omega} = \frac{\omega d_{\text{eff}}}{nc} E_\omega^2 L \frac{\sin(\Delta k L/4)}{(\Delta k L/4)} \exp(-i\Delta k L/4). \quad (20)$$

Clearly, the acceptance angle has increased by a factor of two since  $E_{2\omega}$  now reaches zero when  $\Delta k L = 4\pi$ . If we apply the same method to  $N$  crystals of length  $L/N$  with alternating walkoff directions, we find

$$E_{2\omega} = \frac{\omega d_{\text{eff}}}{nc} E_\omega^2 L \frac{\sin(\Delta k L/2N)}{(\Delta k L/2N)} \exp(-i\Delta k L/2N), \quad (21)$$

so the acceptance angle is  $N$  times that of a single crystal of length  $L$ .

The discussion of acceptance angle for parametric processes is applicable to a low peak-gain approximation where  $G_s \lesssim 100$ , with negligible pump depletion. In this case, evolution of the phases is dominated by the phase mismatch  $\Delta k$ . For fixed values of  $\Delta k$  and crystal lengths  $L_{1,2}$ , reversal of the phase rotation  $\Delta k z$  in the second crystal by walkoff compensation increases the effective interaction length and the acceptance angle, as shown in Fig. 4(a) along the slope  $-1$  axis. As the parametric gain increases, we find that the central gain peak of Fig. 4(a) first broadens along the slope  $+1$  axis and narrows along the slope  $-1$  axis, making the central peak nearly round. As the gain is further increased, the peak broadens along both axes and remains nearly round, implying that walkoff compensation offers little or no increase in acceptance angle at very high parametric gain. At high gain the phases of the three waves are continually adjusted by the parametric gain to maintain a phase difference  $\phi_p - \phi_s - \phi_i \approx -\pi/2$ . This adjustment takes place in a length much less than the crystal length. Consequently, the change in the sign of  $\Delta k$  between crystals is relatively

insignificant, implying that the acceptance angles along the two axes are nearly the same.

## 5. TWO-CRYSTAL SINGLE-PASS PARAMETRIC-GAIN MEASUREMENTS

We have verified that the sign of  $d_{\text{eff}}$  changes with crystal orientation for mixing with a single e wave as described in Section 3 by measuring single-pass parametric gain for various orientations of two KTP crystals and by adjusting the intercrystal phase shift. Figure 5 is a diagram of the laboratory apparatus. The crystals were 10 mm long, with antireflection coatings at the pump and the signal wavelengths, and had cut angles of  $\theta = 58^\circ$  and  $\phi = 0^\circ$  to allow phase matching in the  $XZ$  plane with an e-polarized signal (800 nm) and o-polarized pump (532 nm) and idler (1588 nm). For propagation in the  $XZ$  plane of these biaxial crystals, the o-polarization direction is parallel to the  $Y$  axis and the e-polarization direction lies in the  $XZ$  plane.

We measured  $d_{\text{eff}}$  values of 3.0 pm/V and 2.2 pm/V, respectively, for crystals 1 and 2, compared with a value of 3.07 pm/V expected from the best published value.<sup>19</sup> The low  $d_{\text{eff}}$  for crystal 2 appears to be associated with small regions of ferroelectric domain reversal in the crystal. The sign of  $d_{\text{eff}}$  is reversed in these regions, leading to a reduction in net mixing efficiency. The presence of reversed domains was deduced by comparing measured and calculated curves of parametric gain as a function of phase mismatch  $\Delta k$ . Multiple-domain crystals have signatures that range from a single broadened peak centered about  $\Delta k = 0$  to two well-separated peaks, but these parametric-gain signatures are not unique to a specific domain structure. Crystal 2 has a broadened central peak, presumably due to reversed domains of unknown number and length.

The pump light was the second harmonic from an injection-seeded, spatially filtered Nd:YAG laser with pulse energies up to 12 mJ and a pulse duration of 7 ns FWHM. A spatially filtered, single-longitudinal-mode 800-nm cw diode laser provided a 30-mW input signal

beam. The pump and the signal beam diameters were 2.5 mm and 1.5 mm, respectively, at their  $1/e^2$  irradiance points. The 0.49-mm displacement of the signal beam due to walkoff, in opposite directions in each crystal, had a negligible effect on the mixing efficiency. With the aid of a beam-profiling video camera, the pump and the signal beams were carefully collimated and overlapped. When the crystals were placed in the beams and rotated to the angles of highest signal gain, the peak pump fluence of  $0.25 \text{ J/cm}^2$  gave a typical single-crystal single-pass gain of 6. Pump depletion was negligible.

Gain surfaces were recorded on a  $\Delta k_1, \Delta k_2$  grid by individually locating  $\Delta k_1 = 0$  and  $\Delta k_2 = 0$  as accurately as possible and then rotating each crystal over a range of  $\Delta k$  values. The crystals were rotated about the  $Y$  axis by stepping motors with an external angular resolution of  $78.5 \mu\text{rad}$ , corresponding to an internal angular resolution of  $43.5 \mu\text{rad}$ , or steps of  $\Delta kL/\pi = 0.093$ . The grids consisted of  $40 \times 40$  or  $40 \times 50$  points, depending on the orientation of the second crystal, with one or two stepping motor steps between each point. Three laser pulses were averaged to produce the gain recorded at each grid point. This procedure was repeated three times, as the second crystal was placed first in the correct orientation, then in the  $d_{\text{eff}}$ -reversed, or incorrect orientation, and finally in the  $d_{\text{eff}}$ -reversed orientation with a phase-correction plate inserted between the crystals. A phase shift of any odd integral multiple of  $\pi$  will correct the intercrystal phase. The phase plate in this experiment was an uncoated 100- $\mu\text{m}$ -thick optically flat window of BK7 glass that produced a total phase shift of approximately  $4.6\pi$ .

To find the parametric gain at a single, well-defined value of pump irradiance, we recorded the gain only at the center of the pump beam and at the peak of the pump pulse. A computer-controlled data-acquisition system recorded the input cw signal irradiance, the peak amplified signal irradiance, and the incident and transmitted peak pump irradiances for individual laser pulses. As shown in Fig. 5, we took great care to ensure that the 800-nm signal alone reached the signal detector. The peak irradiances of the pump and the amplified signal pulses were acquired by detectors with bandwidths of  $\sim 1 \text{ GHz}$  connected to fast samplers with gate widths of 200 ps. Timing jitter of the 200-ps gates with respect to the pump and the signal pulses was effectively eliminated by triggering the fast samplers with a constant-fraction discriminator, triggered in turn by the pump pulse with a 200-ps rise-time photodiode. A 525- $\mu\text{m}$ -diameter aperture in the signal beam ensured that the gain of the signal was measured only for the small central portion of the interacting beams where the pump-beam irradiance and the signal gain were nearly uniform.

Figures 6(a) and 7(a) show results of the single-pass parametric-gain measurements for correct and incorrect crystal orientations, along with the corresponding surfaces predicted from Eq. (16) in Figs. 6(b) and 7(b). Measured results for the partially phase-corrected case are shown in Fig. 6(c). The measured gain surfaces show good qualitative agreement with the calculated gain, but there are differences such as the magnitude of the gain and asymmetry between the secondary gain peaks along the  $\Delta k_1 = 0$  and  $\Delta k_2 = 0$  directions. For the correct, in-

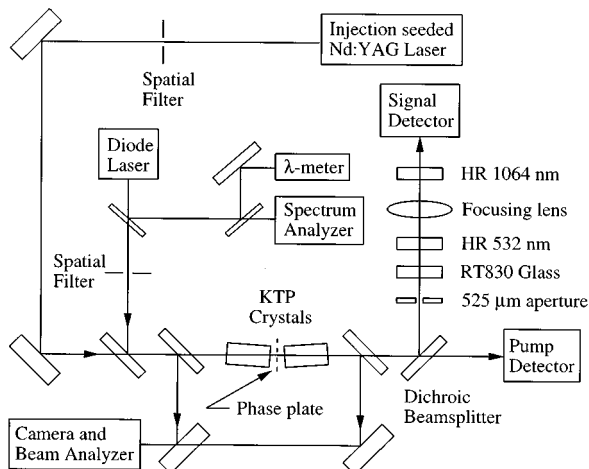


Fig. 5. Experimental arrangement for two-crystal, single-pass parametric-gain measurements. HR, highly reflective.

correct, and incorrect-with-phase-plate orientation, the pulse-averaged peak pump irradiances were  $4.0 \times 10^{11}$  W/m<sup>2</sup>,  $5.9 \times 10^{11}$  W/m<sup>2</sup>, and  $6.1 \times 10^{11}$  W/m<sup>2</sup>, respectively, yielding calculated peak gains of 16.8, 11.5, and 28.6 compared with measured gains of 12.1, 6.5, and 24.8. Although measured quantities were used in Eq. (16) whenever possible, a detailed comparison of experiment and calculation is beyond the scope of this paper. Some of the discrepancy may arise from small, unmeasured intercrystal phase shifts introduced by antireflective coatings, from reflective losses at the crystal surfaces, and from the unknown domain structure of crystal 2. Clearly, the qualitative features of the calculation and the

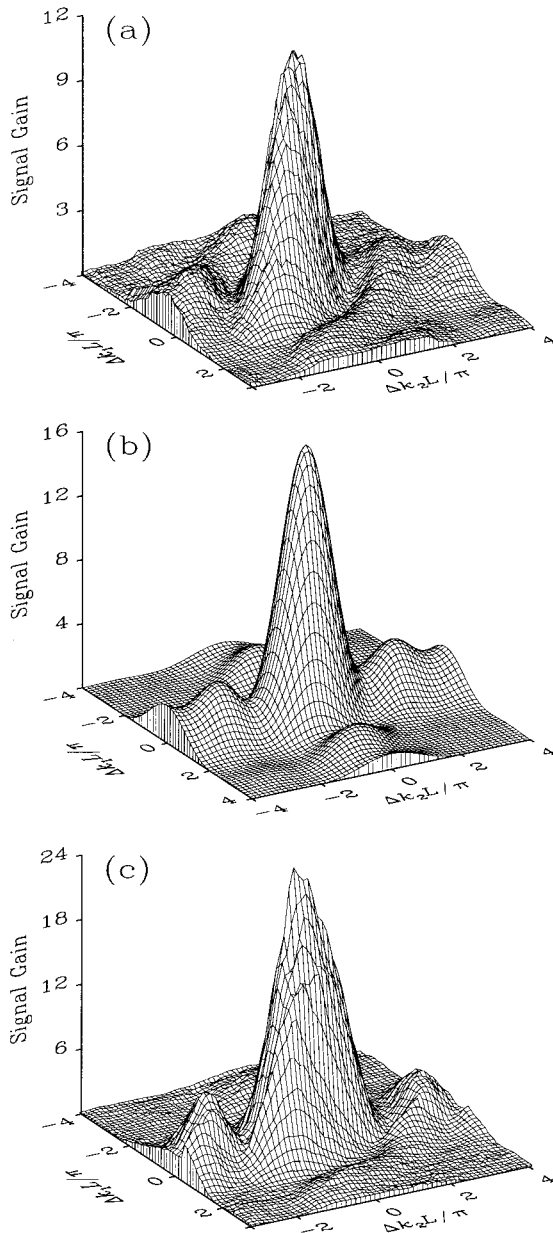


Fig. 6. Two-crystal, single-pass parametric gain. (a) Measured and (b) calculated with Eq. (16), the crystals are oriented so the signs of  $d_{\text{eff}}$  are the same. (c) For the measured gain the signs of  $d_{\text{eff}}$  are opposite, but a phase-correction plate is inserted between the crystals. Pump fluence and the resulting gain in (c) are larger than in (a).

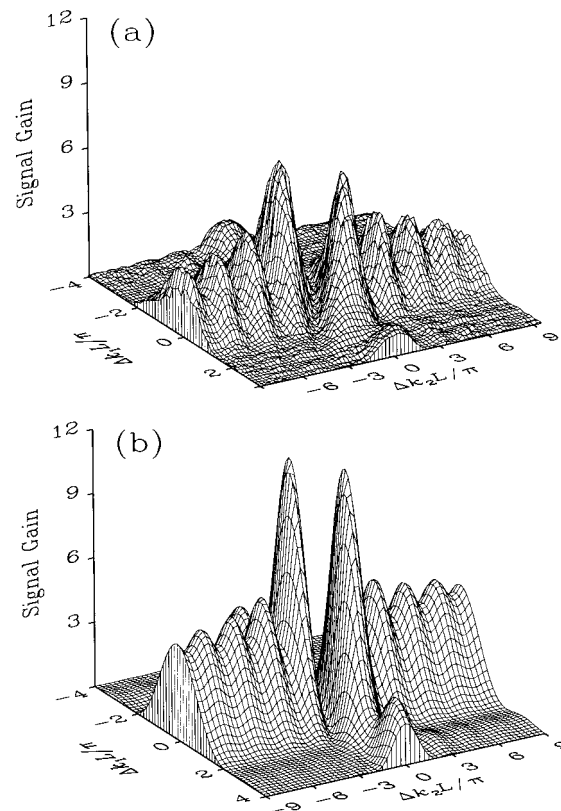


Fig. 7. Two-crystal, single-pass parametric gain with crystals oriented so the signs of  $d_{\text{eff}}$  are opposite. (a) Measured and (b) calculated with Eq. (16).

experiment are in good agreement. The sign of  $d_{\text{eff}}$  changes as predicted for various crystal orientations.

## 6. TWO-CRYSTAL PARAMETRIC OSCILLATION

It is interesting to consider the behavior of a parametric oscillator based on two walkoff-compensating crystals. This is of considerable practical interest because in addition to counteracting walkoff to allow better beam overlap, it also avoids the problem of beam translation as the crystal angles are changed to tune the wavelength, and the increased acceptance angle may also be beneficial. As we discussed above, it is always possible to optimize the parametric gain by setting  $\Delta k_1 = \Delta k_2 = 0$  and adjusting the intercrystal phase. This positions the operating point at the point of highest gain on the surface shown in Fig. 1(a). The device should then behave much like a single-crystal oscillator with a crystal length of  $2L$  and  $\Delta k = 0$ . However, if we attempt to operate at some other point on the gain surface, or if we use the incorrect orientation, the behavior is more difficult to predict. How would the beam quality, efficiency, and other characteristics be affected in such a situation? Further, how easy is it in practice to find the point of maximum gain?

In this section we investigate these questions theoretically and experimentally for one particular oscillator design. Our experimental layout is diagrammed in Fig. 8. The oscillator uses two 10-mm-long KTP crystals, antireflection coated at the pump and the signal wavelengths,

with the same polarizations as those in the single-pass gain measurements. This pair of crystals, cut at  $\theta = 51^\circ$ , had closely matched  $d_{\text{eff}}$  values with measured values<sup>19</sup> of 3.05 pm/V for crystal 1 and 2.92 pm/V for crystal 2. As in the single-pass measurements, the crystals are rotated with stepping motors but with a higher internal angular resolution of 21  $\mu\text{rad}$ , equivalent to steps of  $\Delta kL/\pi = 0.045$ . The crystals were placed in either the correct or the incorrect orientation, and a phase-correction plate was used to change quickly to net-incorrect or net-correct orientations, respectively. The phase corrector was an antireflection-coated, optically flat, 125- $\mu\text{m}$ -thick fused-silica window with a total phase shift of almost exactly  $5\pi$  and transmissions  $T_{800\text{nm}} > 98\%$ ,  $T_{1588\text{nm}} > 98\%$ , and  $T_{532\text{nm}} \geq 80\%$ . A ring cavity composed of three flat mirrors resonated only the signal wave. It had a length of approximately 14 cm and an output coupler reflectance of  $\sim 84\%$  at 800 nm. The ring plane was parallel to the critical plane of the crystals. A lock-in stabilizer and a piezoelectric mirror mount maintained a cavity length that resonated the 800-nm seed light during seeded operation. The pump and the injected signal beams had  $1/e^2$  diameters of approximately 1.2 mm, and the pump wave was carefully aligned along the cavity axis. To examine the signal spectrum, we used a video camera in conjunction with a diffraction grating, as shown in Fig. 8. Minimum measurable frequency shifts with this arrangement were  $\sim 50$  GHz. This resolution was usually adequate since the acceptance bandwidth of the KTP crystals was  $\sim 9$   $\text{cm}^{-1}$ . In most cases, seeded and unseeded oscillations were easily distinguished by simply blocking and unblocking the seed beam. However, given the low resolution, we could not detect effects such as small shifts from the seed frequency during seeded operation owing to small nonzero  $\Delta k$ .<sup>20</sup> The video camera was also used to look for tilts or beam distortions by imaging the far-field signal fluence pattern created by a 1-m focal-length lens.

We will continue to use the single-pass gain surfaces generated by Eq. (16) in Figs. 1 and 2 to discuss phase mismatch, crystal orientation, and intercrystal phase effects but emphasize that the approximation of negligible pump depletion is appropriate only below the oscillation

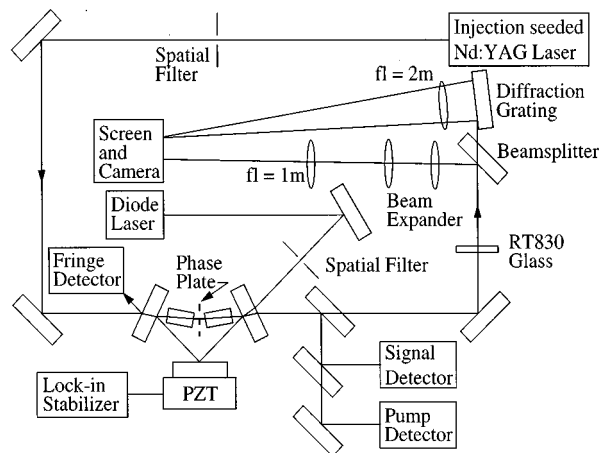


Fig. 8. Experimental arrangement for two-crystal optical parametric oscillator measurements. PZT, piezoelectric transducer.

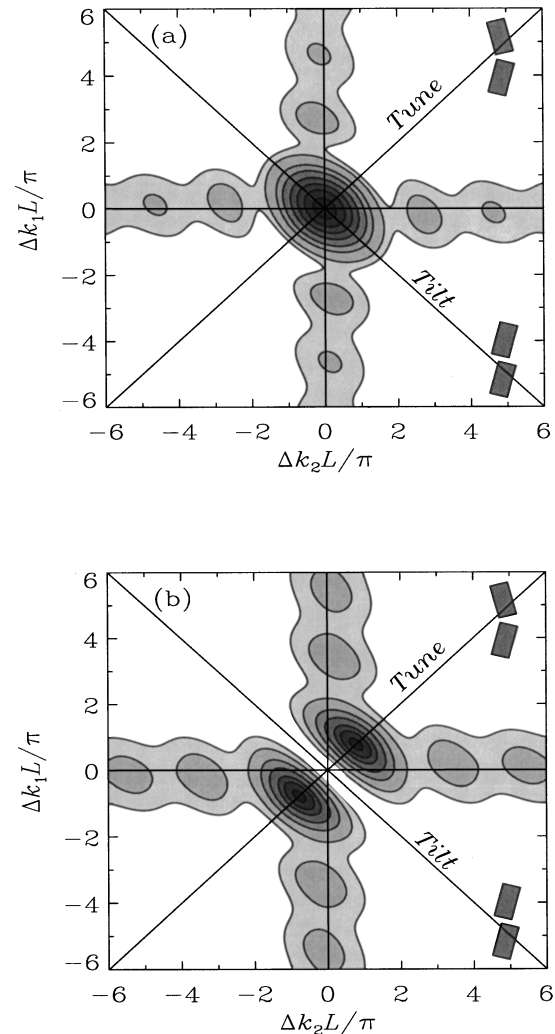


Fig. 9. Contour plots of calculated two-crystal, single-pass parametric gain. Crystal rotations for “Tune” and “Tilt” behavior exhibited by the two-crystal walkoff-compensated oscillator are indicated on the diagonal axes. (a) Crystals are oriented so the signs of  $d_{\text{eff}}$  are the same. (b) Crystals are oriented so the signs of  $d_{\text{eff}}$  are opposite.

threshold. Above threshold we rely on our numerical model of OPO’s. It is a model of nanosecond, injection-seeded oscillators that uses beams with Gaussian spatial and temporal profiles and includes all relevant cavity parameters, walkoff, diffraction, and pump depletion. It has been carefully validated in earlier work.<sup>21</sup>

### A. Beam Tilt

We first note that the single-pass gain surfaces plotted in Figs. 1 and 2 are for collinear plane waves and for a particular set of monochromatic wavelengths. If the beams tilt or the wavelengths shift, the values of  $\Delta k$  change. As we discussed above, if we adjust the crystal angles for a particular value of  $(\Delta k_1, \Delta k_2)$  for the nominal direction and wavelengths, but then tilt the e-polarized signal wave slightly in the critical plane, the value of  $\Delta k_1$  shifts by an amount proportional to the tilt, while  $\Delta k_2$  shifts by an equal amount in the opposite direction. Thus tilts of the

signal wave tend to translate the  $(\Delta k_1, \Delta k_2)$  coordinate along lines parallel to that labeled "Tilt" in Figs. 9(a) and 9(b), which are contour plots of Figs. 1(a) and 1(b) with  $A_1B_1 = A_2B_2 = 1.49 \times 10^4 \text{ m}^{-2}$ . This suggests that if we adjust the crystals to the point  $\Delta k_1L/\pi = 1, \Delta k_2L/\pi = -1$  (1, -1) in Fig. 9(a), well off the gain maximum, the

e-polarized signal wave might tilt to seek out the region of highest gain at (0, 0). An alternative way of viewing this is to note that the point (1, -1) corresponds to tilting both crystals in the same direction, as indicated in Figs. 9(a) and 9(b) by the diagram of the two crystals in the lower right corner. With this set of crystal tilts, the angle of

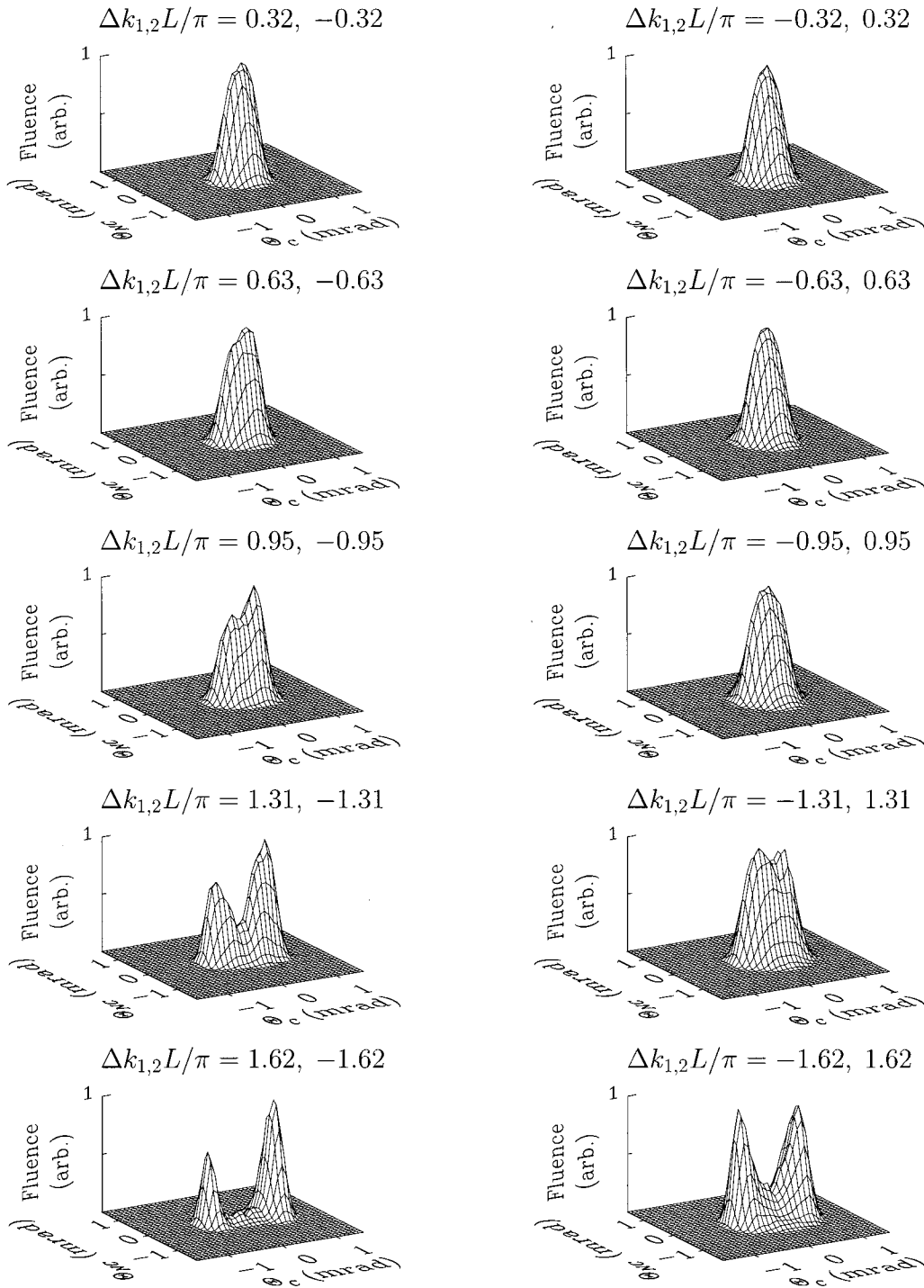


Fig. 10. Measured far-field signal-fluence profiles for increasing values of  $\Delta k_1L/\pi, \Delta k_2L/\pi$  plotted against the critical and the non-critical divergence angles  $\Theta_C$  and  $\Theta_{NC}$  with the crystals oriented so the signs of  $d_{\text{eff}}$  are the same. The peak fluence for each profile is normalized to 1. In the left column the range of  $\Delta k_1L/\pi, \Delta k_2L/\pi$  is from 0.32, -0.32 to 1.62, -1.62 ( $\Delta k_1, \Delta k_2 = 1, -1$  to 5, -5  $\text{cm}^{-1}$ ). In the right column the range is the same, but the signs of  $\Delta k_1L/\pi, \Delta k_2L/\pi$  are reversed.

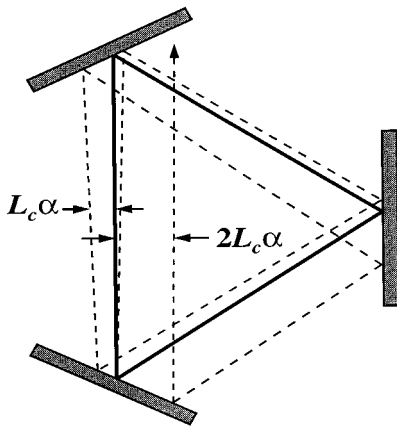


Fig. 11. Path taken by a tilted e-polarized wave in the two-crystal walkoff-compensated three-mirror ring OPO cavity.  $L_c$  is the cavity length, and  $\alpha$  is the tilt angle.

optimum index match, and thus of maximum gain, for the signal wave is tilted by the same amount and in the same direction as the two crystals. Thus we might anticipate that if the two crystals are tilted in the same direction, the signal wave generated in the oscillator will also tilt in that direction. Of course, the cavity tends to counteract such tilts because it favors signal rays aligned along the cavity axis.

We have demonstrated this tilt effect in the laboratory. In the first experiment we used the correct crystal orientation and looked for tilts when operating at various points on the  $\Delta k$  grid. For positions along the tilt line, with values of  $|\Delta k_1 L/\pi| = |\Delta k_2 L/\pi| \geq 0.63$ , we did indeed find tilts of the signal wave, in spite of the fact that tilted waves do not truly resonate in the cavity. As anticipated, the size of the tilts increased with the distance from the  $\Delta k_1, \Delta k_2$  origin. Figure 10 shows measured far-field signal-fluence profiles plotted against the critical and the noncritical divergence angles  $\Theta_C$  and  $\Theta_{NC}$ , taken at pump energies  $\sim 10\%$  above threshold, for increasing  $\Delta k_1 L/\pi, \Delta k_2 L/\pi$ . Double lobes appear in the walkoff direction because the three-mirror ring cavity inverts the beam image in the critical direction on each round trip. A tilted beam follows the path shown in Fig. 11. On alternating passes through the crystals it is tilted clockwise and experiences gain. On the other passes it is tilted counterclockwise and has little gain. It also walks away from the central axis of the cavity where the pump beam lies. The beams tilted clockwise and counterclockwise comprise the two far-field lobes that we observe. Not surprisingly, the separation of the two lobes is approximately twice the tilt of the two crystals divided by the refractive index of the crystals.

In another experiment we used the incorrect orientation and explored behavior near the tilt line shown in Fig. 9(b). We found that if we were exactly on the line, the signal wave had a tilt but its frequency was shifted more than 50 GHz from the seed frequency. If we deviated from the line by a small amount, we had tilt and seeding, with oscillation at the seed frequency verified as usual by blocking and unblocking the seed. This meets expectations because from a position exactly on the tilt line, a tilt

alone would lead to the no-gain valley on the gain surface, whereas from a position off the line a tilt would lead to a position near one of the central gain peaks.

These tilts are present whether the oscillator is seeded or unseeded. In contrast, for a single-crystal oscillator, we have observed tilts for seeded operation but not for unseeded operation. In the walkoff-compensated case, however, the two crystals are attempting to tune the wavelength in opposite directions. In fact, we found that if we operated along the tilt line with sufficiently large crystal tilts, oscillation ceased at the seed wavelength and instead occurred at two simultaneous signal wavelengths corresponding to index matching in the individual crystals. The crystals were acting independently in this case, each supporting oscillation at its angle-tuned wavelength. The device was operating on the  $\Delta k_1 = 0, \Delta k_2 = 0$  ridges of the gain surface that correspond to single-crystal gain.

We should point out that the tilts we observe are more a curiosity than a serious concern in applying walkoff-compensated oscillators because the tilts are significant only for values of  $\Delta k$  large enough that the parametric gain is noticeably reduced. Thus if the crystal angles are carefully adjusted to minimize the pump threshold energy, the tilts should be quite small. This may not be the case if the ring plane is perpendicular to the critical plane. In that case there will be only a single lobe because the beam image reversal occurs only in the ring plane. In fact, our model indicates that for this arrangement the beam tilts by approximately the tilt of the crystals divided by their refractive index even for small tilts with the correct orientation. The model also predicts a small signal beam tilt for the incorrect orientation at the maximum gain point. This interplay of cavity design and beam tilt may be an issue for applications where precise beam pointing is crucial.

## B. Wavelength Tuning

In contrast to tilts, a wavelength shift of the signal and the idler waves would shift the two  $\Delta k$  values in the same direction. In this case the operating point shifts along a line parallel to the one labeled "tune" in Figs. 9(a) and 9(b). Not surprisingly, movement along this line corresponds to counterrotating the crystals, which is the usual method of tuning the wavelength of walkoff-compensated two-crystal oscillators. We found that when we rotated the correctly oriented crystals so the operating point lay on the tune line of Fig. 9, the oscillation wavelength was that of the seed over a range of approximately  $|\Delta k_1 L/\pi| = |\Delta k_2 L/\pi| < 1$ . Beyond this range of  $\Delta k$  values, the wavelength was determined by the crystal angles rather than the seed. No tilts were observed.

If the incorrect orientation of the crystals is used, we might expect that seeded operation at the  $\Delta k_1 = \Delta k_2 = 0$  point would lead to unseeded oscillation at the two large gain peaks displaced along the tune line. We never observed two-frequency oscillation at the (0, 0) point. We found instead that, as we moved along the tune line, seeded oscillation occurred preferentially on the positive  $\Delta k$  peak with the incorrect orientation and on the negative  $\Delta k$  peak for the net-incorrect orientation (crystals correct, phase-plate inserted), but there was little difference in conversion efficiency either way. We do not fully

understand this tuning behavior. One explanation is that the phase shifts<sup>22</sup> associated with nonzero  $\Delta k$  tend to focus the signal beam for one sign of  $\Delta k$ , reducing the cavity loss and lowering the threshold. Another explanation is that nonzero phase shifts owing to coatings on the crystals introduced asymmetry in the gain peaks, favoring oscillation on the positive  $\Delta k$  peak in the incorrect orientation. The net phase shift of  $\pi$  from the phase plate would then reverse the peak asymmetry in the net-incorrect orientation, favoring oscillation on the negative  $\Delta k$  peak.

### C. Efficiency

On the single-pass gain surfaces the maximum gain is highest for the correct orientation, so we expect this case to have the lowest pump threshold for oscillation. We might also expect it to have the highest conversion efficiency as the pump level rises above the threshold value. This might provide a signature to differentiate between correct and incorrect crystal orientations. We have measured signal energy versus pump energy for seeded and unseeded operation and plot it in Fig. 12. Part (a) shows

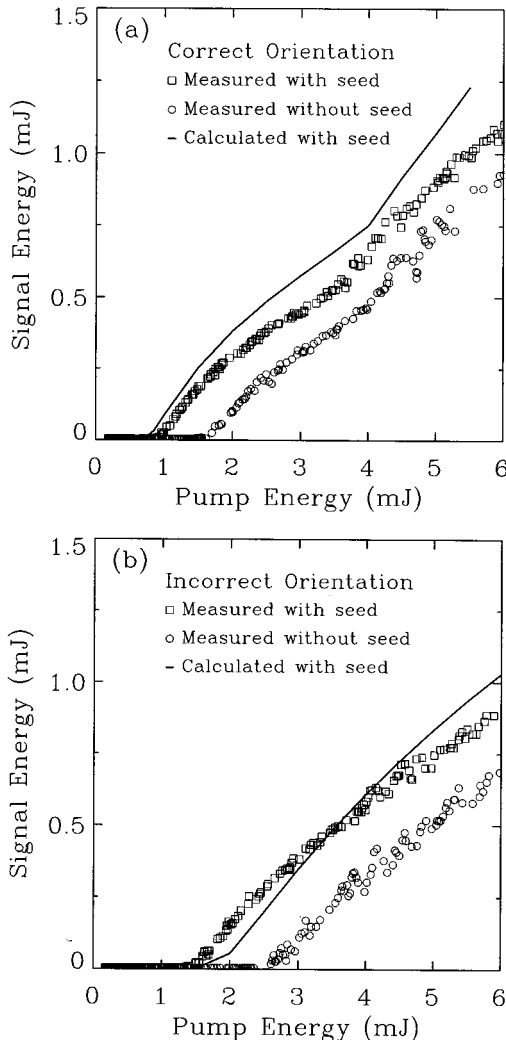


Fig. 12. Signal energy versus pump energy for (a) the correct orientation with  $\Delta k_1 = \Delta k_2 = 0$  and (b) the incorrect orientation with  $\Delta k_1 L/\pi = \Delta k_2 L/\pi \approx -0.45$ .

curves for the correct orientation with  $\Delta k_1 = \Delta k_2 = 0$  for seeded (boxes) and unseeded (circles) operation. Part (b) shows the same for the incorrect orientation (actually crystals correct, phase-plate inserted) with the crystals tuned to  $\Delta k_1 L/\pi = \Delta k_2 L/\pi \approx -0.45$ , to be near a gain peak on the incorrect single-pass gain surface. Although reduced transmission of the pump with the phase plate inserted may exaggerate these results ( $T_{532\text{nm}} \geq 80\%$ ), the figure shows that there is indeed a significant difference in threshold and efficiency between the correct and the incorrect orientations. This holds for seeded or unseeded operation.

The solid curves in Figs. 12(a) and 12(b) were calculated with our numerical model and included transmission properties of the phase plate and the crystals. For the correct orientation the calculated efficiency is greater overall than the measured efficiency, but the calculated and the measured shapes agree reasonably well, including a small change in the slope of the efficiency curve near a pump energy of  $\sim 4$  mJ. For the incorrect orientation the shapes again agree reasonably well, but the calculated threshold and slope of the efficiency curve are both greater than the measured result. In any event the model predicts an increase of a factor of  $\sim 2$  in threshold between correct and incorrect orientations, and the experiment demonstrates an increase of a factor of  $\sim 1.5$  for both seeded and unseeded cases. This is a large effect and a clear signature of crystal orientation.

### D. Beam Quality

We showed in earlier work that nonzero  $\Delta k$  can lead to frequency shifts in injection-seeded optical parametric oscillators<sup>20</sup> and to phase distortions in frequency mixing.<sup>22</sup> Because the incorrect orientation requires operation at nonzero  $\Delta k$  values, we might expect the transverse mode quality and the spectrum to be degraded compared with an oscillator based on the correct crystal orientation. In fact there seems to be little difference in beam quality between the two cases in our model and in the laboratory. Figure 13 shows measured and calculated far-field signal-fluence profiles with a pump energy of 6 mJ (peak irradiance of  $\sim 1.4 \times 10^{12}$  W/m<sup>2</sup>). Figures 13(a) and 13(b) show the measured and the calculated profiles, respectively, for seeded operation with the correct orientation at  $\Delta k_1 = \Delta k_2 = 0$ . The structure observed in the wings of these profiles is typical of high-output OPO operation, with the pump energy 5–6 times above threshold. Figures 13(c) and 13(d) show measured and calculated profiles, respectively, for seeded operation with the incorrect orientation at  $\Delta k_1 L/\pi = \Delta k_2 L/\pi = -0.45$ . Here the pump energy is 3–4 times above threshold, and we observe a slight increase in width in these profiles compared with the correct orientation. Finally, Fig. 13(e) shows the same measured profile as in Fig. 13(c) but for unseeded operation. At only 2–2.5 times above threshold this unseeded profile is narrower than its more efficient, seeded counterpart.

Although we did not examine the laboratory spectra with high resolution, our model indicates that, for seeded operation, the correct and the incorrect orientations are similar and nearly transform limited. Thus there ap-

pears to be little difference in beam quality or spectral purity between the correct and the incorrect cases.

### E. Practical Considerations

We have shown that to obtain optimum performance from a two-crystal device, it is necessary to design it so the nonlinear coefficients are effectively the same sign in the two crystals. The issue then is how to tell when this is achieved. The only clear signatures are the single-pass gain surfaces and the conversion efficiency. As a practical matter, we find that a cw seed laser is the most useful diagnostic tool available. The two cases can be distin-

guished easily from single-pass gain or somewhat more tediously from seeded oscillation thresholds and efficiency. One procedure to determine the correct orientation from single-pass gain is to first phase match one crystal at  $\lambda_{\text{seed}}$  and then tune the second crystal through  $\Delta k = 0$ . The signatures are distinct: For the correct orientation, a single strong gain peak is observed; for the incorrect orientation, two approximately symmetric peaks are observed.

Although such single-pass gain measurements are by far the simplest method for distinguishing correct from incorrect crystal orientation, we have also deduced it from

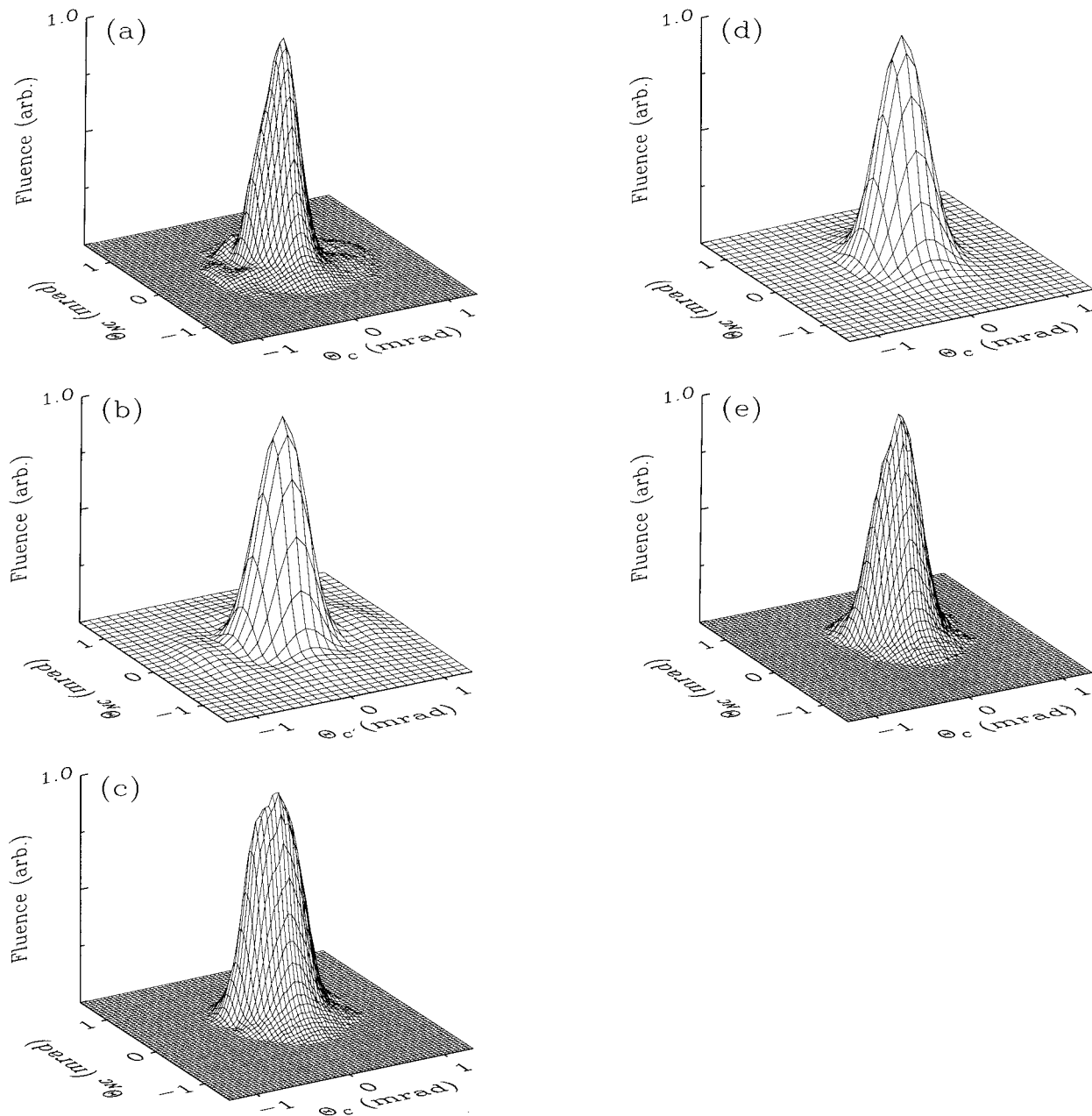


Fig. 13. Far-field signal-fluence profiles with 6 mJ of pump energy plotted against the critical and the noncritical divergence angles  $\Theta_C$  and  $\Theta_{NC}$ . The peak fluence for each profile is normalized to 1. (a) Measured, seeded, correct orientation,  $\Delta k_1 = \Delta k_2 = 0$ . (b) Calculated, same as (a). (c) Measured, seeded, incorrect orientation,  $\Delta k_1 L/\pi = \Delta k_2 L/\pi \approx -0.45$ . (d) Calculated, same as (c). (e) Same as (c) but unseeded.

seeded, near-threshold oscillation by angle tuning the crystals to move along the tune lines in Figs. 9(a) and 9(b). With the pump power adjusted to just above the oscillation threshold, with barely observable oscillation occurring at the peak(s) of the correct and the incorrect gain surfaces, the incorrect orientation reaches threshold over the two regions of the tune curve associated with the two gain peaks, whereas the correct orientation reaches threshold over only one region. Without a seed laser, orientation could probably be determined from the correct and the incorrect unseeded oscillation thresholds as indicated Fig. 12, but our experience indicates that this may be difficult. With a seed laser the OPO cavity can be aligned interferometrically by sweeping the cavity length and observing transmission étalon fringes, and the pump beam can be precisely overlapped with the cavity mode with the help of a beam profiler. A distinct difference in oscillation thresholds may not be observed without these useful diagnostics, particularly for ring cavities.

A phase-correction plate provides yet another method of determining crystal orientation in a seeded oscillator. If the orientation is correct and the crystals are carefully adjusted to the point of minimum threshold, oscillation will stop when the phase plate is inserted between the crystals, and it cannot be restored by adjusting  $\Delta k_1$ ,  $\Delta k_2$ . If the orientation is incorrect, we find that the output power may actually increase when the plate is inserted, and by adjusting  $\Delta k_1$  and  $\Delta k_2$ , output power will usually increase even more. This behavior was easily observed in our seeded two-crystal oscillator. Observations of such near-threshold behavior convinced us that locating the point  $\Delta k_1 = \Delta k_2 = 0$  was more reliably achieved from minimizing the oscillation threshold than from maximizing the signal power at pump fluences well above threshold.

Finally, if a two-e-wave process with identically cut crystals forces the use of a phase-correction plate, the plates do have some drawbacks. A plate without antireflection coatings has the transmission characteristics of a low-finesse étalon. Antireflection coatings can enhance transmission but may introduce additional phase shifts, and it may be difficult to achieve low reflectivity over broad tuning ranges. In addition, the plates must be thin to produce the net phase shift of  $\pi$  over a wide range of wavelengths. Consequently, they are fragile.

## 7. CONCLUSIONS

We have shown both mathematically and by laboratory measurements that parametric gain in two-crystal devices depends sensitively on the relative signs of  $d_{\text{eff}}$  for the two crystals, on the intercrystal phase shift, and on the values of  $\Delta k_1$  and  $\Delta k_2$ . We showed that the gain is maximized when the crystals have the same sign for  $d_{\text{eff}}$  if the intercrystal phase shift is zero or when the signs are reversed if the phase shift is  $\pi$ . The lowest gain occurs when the signs are opposite and the phase shift is zero or when the signs are the same but the phase shift is  $\pi$ . In this case the peak gain lies not at  $\Delta k_1 = \Delta k_2 = 0$  but near  $\Delta k_1 L/\pi = \Delta k_2 L/\pi = \pm 1$ , where  $L$  is the length of each crystal. We also showed how the orientations and the crystallographic cuts of the crystals determine the

relative signs of the  $d_{\text{eff}}$  values as well as the direction of birefringent walkoff. The acceptance angle was also shown to increase for walkoff-compensated arrangements of multiple crystals.

The performance of one particular two-crystal, walkoff-compensated optical parametric oscillator was examined in the laboratory and by use of a detailed numerical model. We demonstrated beam tilts associated with certain values of  $\Delta k$  that are unique to two-crystal devices. We also found that when the sign of the nonlinearity in the two crystals was opposite, the efficiency was reduced. However, the sign reversal seemed to have little influence on the spectral purity when the oscillator was seeded or on the far-field beam profiles. We conclude that to achieve optimum performance of the oscillator, it is necessary to find the correct crystal orientation, but the incorrect orientation also gives acceptable performance if efficiency is not critical. We have not analyzed oscillators with other combinations of e and o waves or other cavity configurations, but we hope we have provided the framework for such analysis and for future development of walkoff-compensated devices.

## ACKNOWLEDGMENTS

We thank Ron Blachman of Crystal Technology, Inc., for helpful discussions of crystallographic orientation and signs of  $d_{\text{eff}}$ . This research is supported by the U.S. Department of Energy under contract DE-AC04-94AL85000.

## REFERENCES

1. V. D. Volosov, A. G. Kalintsev, and V. N. Krylov, "Degenerate parametric processes in three-wave interactions in tandem crystals," *Sov. Tech. Phys. Lett.* **2**, 32–34 (1976).
2. V. D. Volosov, A. G. Kalintsev, and V. N. Krylov, "Suppression of degenerate parametric processes limiting frequency-doubling efficiency of crystals," *Sov. J. Quantum Electron.* **6**, 1163–1167 (1976).
3. V. D. Volosov and A. G. Kalintsev, "Optimum optical second-harmonic generation in tandem crystals," *Sov. Tech. Phys. Lett.* **2**, 373–375 (1976).
4. V. D. Volosov, A. G. Kalintsev, and V. N. Krylov, "Phase effects in a double-pass frequency doubler," *Sov. Tech. Phys. Lett.* **5**, 5–7 (1979).
5. R. B. Andreev, K. V. Vetrov, V. D. Volosov, and A. G. Kalintsev, "Three-wave parametric processes in multicrystal nonlinear frequency converters," *Opt. Spectrosc.* **65**, 90–93 (1988).
6. B. Ya. Zel'dovich, Yu. E. Kapitskii, and A. N. Chudinov, "Interference between second harmonics generated in two different KTP crystals," *Sov. J. Quantum Electron.* **20**, 1120–1121 (1990).
7. M. Watanabe, K. Hayasaka, H. Imajo, and S. Urabe, "Continuous-wave sum-frequency generation near 194 nm with a collinear double enhancement cavity," *Opt. Commun.* **97**, 225–227 (1993).
8. L. K. Samanta, T. Yanagawa, and Y. Yamamoto, "Technique for enhanced second harmonic output power," *Opt. Commun.* **76**, 250–252 (1990).
9. W. R. Bosenberg, W. S. Pelouch, and C. L. Tang, "High-efficiency and narrow-linewidth operation of a two-crystal  $\beta$ -BaB<sub>2</sub>O<sub>4</sub> optical parametric oscillator," *Appl. Phys. Lett.* **55**, 1952–1954 (1989).
10. J. Zondy, M. Abed, and S. Khodja, "Twin-crystal walk-off-compensated type-II second-harmonic generation: single-pass and cavity-enhanced experiments in KTiOPO<sub>4</sub>," *J. Opt. Soc. Am. B* **11**, 2368–2379 (1994).

11. J.-J. Zondy, "Experimental investigation of single and twin AgGaSe<sub>2</sub> crystals for cw 10.2  $\mu$ m SHG," *Opt. Commun.* **119**, 320–326 (1995).
12. M. A. Norton, D. Eimerl, C. A. Ebbers, S. P. Velsko, and C. S. Petty, "KD\*P frequency doubler for high average power applications," *Proc. SPIE* **1223**, 75–83 (1990).
13. S. E. Harris, "Method to lock an optical parametric oscillator to an atomic transition," *Appl. Phys. Lett.* **14**, 335–337 (1969).
14. A. Yariv, *Introduction to Optical Electronics* (Holt, Rinehart, & Winston, New York, 1976).
15. R. W. Boyd, *Nonlinear Optics* (Academic, Boston, Mass., 1992).
16. Y. R. Shen, *The Principles of Nonlinear Optics* (Wiley, New York, 1984).
17. F. Zernike and J. E. Midwinter, *Applied Nonlinear Optics* (Wiley, New York, 1973).
18. V. G. Dmitriev, G. G. Gurzadyan, and D. N. Nikogosyan, *Handbook of Nonlinear Optical Crystals* (Springer-Verlag, New York, 1991).
19. D. J. Armstrong, W. J. Alford, T. D. Raymond, and A. V. Smith, "Absolute measurement of the effective nonlinearities of KTP and BBO crystals by optical parametric amplification," *Appl. Opt.* **35**, 2032–2040 (1996).
20. T. D. Raymond, W. J. Alford, A. V. Smith, and M. S. Bowers, "Frequency shifts in injection-seeded optical parametric oscillators with phase mismatch," *Opt. Lett.* **19**, 1520–1522 (1994).
21. A. V. Smith, W. J. Alford, T. D. Raymond, and M. S. Bowers, "Comparison of a numerical model with measured performance of a seeded, nanosecond KTP optical parametric oscillator," *J. Opt. Soc. Am. B* **12**, 2253–2267 (1995).
22. A. V. Smith and M. S. Bowers, "Phase distortions in sum- and difference-frequency mixing in crystals," *J. Opt. Soc. Am. B* **12**, 49–57 (1995).